
Masters Theses

Student Theses and Dissertations

Spring 2018

Embedded fiber optic sensors for temperature monitoring of continuous casting mold

Yiyang Zhuang

Follow this and additional works at: https://scholarsmine.mst.edu/masters_theses



Part of the [Electrical and Computer Engineering Commons](#)

Department:

Recommended Citation

Zhuang, Yiyang, "Embedded fiber optic sensors for temperature monitoring of continuous casting mold" (2018). *Masters Theses*. 7791.

https://scholarsmine.mst.edu/masters_theses/7791

This thesis is brought to you by Scholars' Mine, a service of the Missouri S&T Library and Learning Resources. This work is protected by U. S. Copyright Law. Unauthorized use including reproduction for redistribution requires the permission of the copyright holder. For more information, please contact scholarsmine@mst.edu.

**EMBEDDED FIBER OPTIC SENSORS FOR TEMPERATURE MONITORING
OF CONTINUOUS CASTING MOLD**

by

YIYANG ZHUANG

A THESIS

Presented to the Faculty of the Graduate School of the

MISSOURI UNIVERSITY OF SCIENCE AND TECHNOLOGY

In Partial Fulfillment of the Requirements for the Degree

MASTER OF SCIENCE IN ELECTRICAL ENGINEERING

2018

Approved by

Dr. Jie Huang, Advisor

Dr. Lianyi Chen

Dr. Amardeep Kaur

© 2018

Yiyang Zhuang

All Rights Reserved

ABSTRACT

The continuous casting process has been widely used for most of the steel production in the world instead of conventional ingot casting/rolling. Traditionally, thermocouples are being widely used to monitor the mold temperature in the continuous casting which has the following drawbacks: large size, low spatial resolution, and single detection point. On the contrary, fiber optic sensors can be a promising solution to the continuous casting temperature monitoring owing to its advantage of compact size, high resolution, high-temperature survivability, etc..

In this thesis, we successfully developed extrinsic Fabry-Perot interferometer (EFPI) sensor for point temperature sensing, and optical frequency domain reflectometry (OFDR) system for distributed temperature sensing. We embedded the optical fiber and fiber optic sensors in the copper slide using electrodeposition for continuous high-temperature sensing. The sensing principle and the fabrication of EFPI sensors was discussed. To verify the best method for sensor coating, three different coating methods were applied to optical fiber sensors before embedding. We observed that the sensitivity of embedded EFPI sensor with wax coating has been surprisingly enhanced more than 30 times. An experiment designed monitoring the casting process of aluminum was conducted, showing fast time response of the embedded EFPI sensor. Also the basic working principle, the nonlinear sweep compensation method and the data processing procedure of OFDR system. A calibration experiment of OFDR system was also demonstrated in this thesis. The OFDR system can achieve 1 cm spatial resolution.

ACKNOWLEDGEMENTS

I would like to express my gratitude to all those people who helped me with my research in this two years. First, I am thankful to my advisor, Dr. Jie Huang. I thank him for giving me this opportunity to work in his lab and this project. I could not have finished this project without his valuable advice and support. I would like to thank Intelligent System Center (ISC) of Missouri University of Science and Technology, the sponsors for this project.

I am grateful to Dr. Lianyi Chen, Department of Mechanical and Aerospace Engineering, and Dr. Amardeep Kaur, Department of Electrical and Computer Engineering, for being my committee members.

I own a great deal of gratitude to the cooperator of this project, Raghavender Reddy Jakka, and Dr. Yang Du, who help me a lot during this project.

I would like to thank our lab members: Chen Zhu, Mohammed Farhan Ahmed, Sasi Jothibas, Xiaotong Tang and Bohong Zhang. I would also like to thank my parents and my wife for their support of my research in the USA.

TABLE OF CONTENTS

	Page
ABSTRACT.....	iii
ACKNOWLEDGEMENTS.....	iv
LIST OF ILLUSTRATIONS.....	vii
LIST OF TABLES.....	ix
SECTION	
1. INTRODUCTION.....	1
1.1. BACKGROUND.....	1
1.2. FIBER OPTIC SENSORS FOR TEMPERATURE SENSING.....	1
1.2.1. Single Point Fiber Optic Sensors.....	2
1.2.2. Distributed Fiber Optic Sensors.....	4
1.3. RESEARCH OBJECTIVE.....	6
1.4. THESIS OVERVIEW.....	7
2. EFPI FABRICATION AND MEASUREMENT PRINCIPLE.....	8
2.1. EFPI FABRICATION.....	8
2.2. EFPI MEASUREMENT PRINCIPLE.....	9
3. OFDR MEASUREMENT PRINCIPLE.....	12
3.1. BASIC PRINCIPLE OF OFDR.....	12
3.2. NONLINEAR SWEPT.....	13
3.3. DATA PROCESSING PROCEDURE.....	15
4. EMBEDDING PROCESS AND MEASUREMENT RESULT.....	17

4.1. EMBEDDING PROCESS	17
4.2. EFPI MEASUREMENT	18
4.3. OFDR MEASUREMENT	24
5. CONCLUSION AND FUTURE WORK.....	32
BIBLIOGRAPHY.....	34
VITA	39

LIST OF ILLUSTRATIONS

Figure	Page
1.1. The structure of FPI sensor (a) EFPI (b) IFPI.....	4
2.1. The schematic diagram of EFPI sensor	8
2.2. The microscope image of EFPI sensor	9
2.3. The interference spectrum of an EFPI sensor	10
3.1. The basic principle of OFDR system.....	12
3.2. The nonlinear swept of the tunable laser	14
4.1. The photo of copper slide with embedded optical fiber sensor	18
4.2. The schematic diagram of the setup of EFPI sensor calibration experiment.....	19
4.3. The spectral shift of EFPI sensors with different coating as a function of temperature	20
4.4. The photo of the casting mold	23
4.5. The temperature response of the EFPI sensor and thermocouple as a function of time	24
4.6. The schematic diagram of the OFDR system and the measurement setup.....	25
4.7. The RBS shifts along the optical fiber inside the furnace in different temperature during heating of annealing process	26
4.8. The RBS shift points of the optical fiber as a function of temperature during heating of annealing process.....	27
4.9. The RBS shifts along the optical fiber inside the furnace in different temperature during cooling of annealing process	28
4.10. The RBS shifts along the optical fiber inside the furnace in different temperature during heating experiment	29
4.11. The RBS shift points of the optical fiber as a function of temperature during heating experiment.....	29

4.12. The RBS shifts along the optical fiber inside the furnace in different temperature during cooling experiment	30
4.13. The RBS shift points of the optical fiber as a function of temperature during cooling experiment.....	31

LIST OF TABLES

Table	Page
4.1. EFPI sensitivity with different coating in different temperature	21

1. INTRODUCTION

1.1. BACKGROUND

The continuous casting process has been widely used for most of the steel production in the world instead of conventional ingot casting/rolling for the production of semi-finished steel shape products [1]. Cooling water is circulated in the copper mold, which cools the molten steel thus forming shell near the mold. Shell breakout is one major problem in the continuous casting which causes quality problems such as strand surface appearance, sticker breakout, narrow-face bleed [2]. To avoid shell breakout, heat flux in the mold should be controlled precisely, which involves strict monitoring of the mold temperature [3].

Traditionally, thermocouples are being widely used to monitor the mold temperature in continuous casting [3-5]. The using of thermocouples has the following drawbacks: large size, low spatial resolution, and single detection point. Typically the thermocouples are embedded into casting mold by drilling holes which cannot set the thermocouples very close to the mold surface. Drilling holes also may influence the integrity of the casting mold, so the number of holes that can be drilled is limited.

1.2. FIBER OPTIC SENSORS FOR TEMPERATURE SENSING

Over past decades fiber optic sensors have been studied because of its unique advantages such as immunity to electromagnetics, compact size, light weight, low cost, high accuracy and distributed sensing capability [6]. Fiber optic sensors have been found in various sensing and measurement applications [7-20].

1.2.1. Single Point Fiber Optic Sensors. Among all the developed single-point fiber optic sensors, grating and interferometric are the most widely studied topics [21-27].

Fiber optic grating sensors consist of fiber Bragg grating (FBG) sensors, chirped FBG (CFBG) sensors, tilted FBG (TFBG) sensors, long-period gratings (LPG) sensors and so on. Typically the fiber optic grating sensors are fabricated by creating a systematic refractive RI change in a doped optical fiber using ultraviolet (UV) light, which can be achieved either by an interference pattern between two intense UV light beams or a phase mask [28]. A fiber optic grating sensors can reflect light with a certain wavelength. The shift is related to the effective grating period which is sensitive to temperature, strain, etc.. By analyzing the shift in the reflected signal the desired parameters can be calculated [29]. Having all the aforementioned advantages of fiber optic sensors, it has high sensitivity, and it can be cascaded in one piece of optical fiber to achieve quasi-distributed sensing [22, 23, 30]. Fiber grating sensors have been applied to measure different parameters such as temperature, strain, and vibration [18, 28, 31].

However, fiber optic grating sensors was merely used in high temperature sensing applications. The reason is that the stability of the grating will dramatically decrease in high temperature and the UV-fabricated pattern will be totally erased in 700 °C [28]. Normally the fiber optic grating sensors are used under 200 °C to keep the reflectivity of the grating. Recently Krasilnikov *et al.* developed their mold monitoring system by drilling holes to place twelve optical fibers with cascaded FBG into the shell of casting mold [32]. But the sensors were not positioned very close to the mold-steel surface, and the sensors worked only around 200 °C. So in practical applications it still cannot work in high temperature environment.

Meanwhile, fiber optic interferometric sensors also have attracted a lot of interests in past decades [33-40]. In a fiber optic interferometric sensor, the sensing is achieved by analyzing the interference signal formed by two or more light beams. The optical path difference is arranged to change with the desired external parameters like temperature, strain, etc. Nowadays fiber optic interferometric sensors consist of four typical structures: Fabry-Perot (F-P), Michelson, Mach-Zehnder (M-Z) and Sagnac. Among four typical structures, the Fabry-Perot interferometer (FPI) sensor is a promising candidate for continuous casting mold owing to the advantage of small size, simple structure and easy in-line fabrication which allows two different optical paths using same physical path [41]. The core of FPI is the F-P cavity is a pair of parallel reflectors. When the light is traveling through the F-P cavity, the light will be reflected by both reflectors. And the reflected lights will interfere each other and generate an interference spectrum. Usually two reflectors will be separated by less than 1 mm to optimize the interference signal. The FPI sensors can be classified into two types: intrinsic Fabry-Perot interferometer (IFPI) sensors and extrinsic Fabry-Perot interferometers. Figure 1.1(a) and (b) shows the schematic diagram of EFPI sensors and IFPI sensors. Figure 1.1(a) shows an EFPI sensor. The cavity material is air and it is formed by one piece of cleaved optical fibers and an external reflector supported by the external structure. For an IFPI sensor, which is shown in Figure 1.1(b), the two reflectors will be fabricated inside the optical fiber so the cavity material is glass. The fabrication for EFPI sensors is simple, but EFPI sensors face the challenge of high coupling loss and careful alignment. On the other hand, IFPI sensors can overcome the disadvantage of EFPI sensors, but high-cost equipment such as femtosecond laser [38, 39] or chemicals for etching [37] are required for reflector fabrication. And since the RI difference between

the reflectors and the optical fiber is small, IFPI sensors have a low reflectivity which decrease the signal-to-noise ratio (SNR) of IFPI. In recent years EFPI sensors have been developed for temperature [9], strain [36], RI [11] and displacement sensing [42]. And several methods is proposed to fabricate the cavity of EFPI [13, 41].

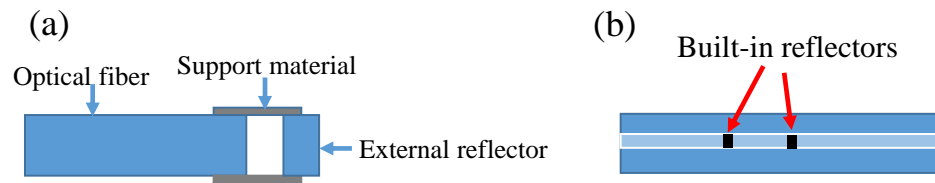


Figure 1.1. The structure of FPI sensor (a) EFPI (b) IFPI

1.2.2. Distributed Fiber Optic Sensors. Single point fiber optic sensors are showing great potential in various sensing applications. However, the number of the sensors that can be used in one system is limited. And an event cannot be detected if it happens between two adjacent sensors.

On the contrary, distributed fiber optic sensors can continuously monitor the events along the whole optical fiber, which attract considerable attention in areas such as structural health monitoring (SMH) and long-distance monitoring [43]. The distributed fiber optic sensing is achieved by detecting the scattering light along the optical fiber. When the incident light is traveling along an optical fiber, the light will be scattered. Depending on the frequency shift of the scattering lights, there exists three kinds of scattering light: Rayleigh, Brillouin and Raman. The RI or physical length of an optical fiber at a position

X will experience variations if external parameters if the optical fiber in this position is influenced by changes in temperature, strain, vibration, etc.. These variations will influence the amplitude and the phase of the backward scattering light. And the distributed sensing can be achieved by detecting and analyzing the backward scattering light [43, 44]. In recent years, several distributed fiber optic sensing techniques have been developed using three kinds of backward scattering [45-50]. Optical time domain reflectometry (OTDR) is the most typical technique among all the developed distributed fiber optic sensing. A light pulse will be sent into a piece of optical fiber. When a light pulse is propagating along the fiber, a small portion of the light will be scattered back and detected. And the location information can be determined by the time that the signal is received. Depending on the type of the detected backward scattering light, there exist three types of OTDR sensors: OTDR sensors, Brillouin OTDR (BOTDR) sensors and Raman OTDR (ROTDR) sensor.

However, the common disadvantage of all the time-domain based distributed fiber optic sensors is the low spatial resolution. The spatial resolution for OTDR sensors can be determined by:

$$\Delta L = \frac{c}{2n_o} \tau \quad (1)$$

where n_o is the RI of the fiber, τ is the width of the light pulse, and c is the speed of light. For conventional OTDR sensors, the spatial resolution is several meters, which is limited by the width of light pulse used for sensing (typically larger than 10 ns). For some applications (e.g., the continuous casting mold temperature monitoring) that require high resolution to precisely monitor the location of events, conventional OTDR is not a suitable solution. To overcome this drawback, Rayleigh backward scattering-based optical frequency domain reflectometry (OFRD) technique has been proposed. Comparing with

conventional OTDR sensors, the OFDR sensors use a tunable laser instead of the laser pulse as the light source. An OFDR sensor can be considered as a series of cascaded FBGs with low reflectivity [17]. When the external parameters change the effective RI or the physical length of optical fiber, the reflection wavelength will shift, and by monitoring the frequency shift, the distributed sensing can be achieved. OFDR provides a promising distributed sensing solution for where high resolution and accuracy are required. With the rapid growth telecommunication industry, high resolution (0.1 pm) and fast tunable lasers (> 10 kHz) and sensitive avalanche photodetectors have become widely available, which fuel the recent surge of distributed fiber sensing using Rayleigh scattering technique. In past decades, OFDR sensors have been studied and proposed in applications like temperature [51], strain [52], vibration [53], RI [17], etc..

1.3. RESEARCH OBJECTIVE

From the discussion above, the main objective of this thesis is to design the sensors that can survive at high temperature and the embedding process.

1. Develop the point optical fiber sensor (EFPI) and the distributed optical fiber sensor (OFDR) that can survive in high temperature.

2. Develop the electrodeposition based embedding method that can embed the EFPI sensors and the normal single-mode optical fiber into the copper slides and protect the optical fiber from copper.

3. Test both EFPI sensor and the OFDR system in high-temperature environment to verify if the sensors can survive in high temperature and compare their temperature response with unembedded sensors.

1.4. THESIS OVERVIEW

The project aims to develop the point optical fiber sensor and distributed optical fiber sensor that can survive the high temperature in steel casting and to develop the embedding technologies that can seamlessly embed the optical fiber sensors inside the copper mold. Two groups co-operated this project. The embedding method is developed by Dr. Lianyi Chen's group. And this thesis will mainly focus on the optical fiber sensor development and the measurement result analysis.

Section 2 focused on the fabrication and the sensing principles of EFPI sensors. The influence of the thermal expansion effect to the sensitivity of the EFPI sensor was discussed.

Section 3 focused the sensing principle and the system structure of OFDR system. The method to compensate the nonlinearity of the tunable laser was discussed. The signal processing method was also introduced.

Section 4 described the embedding process and the test result for optical fiber sensors. The sensitivities of the EFPI sensors with different coating was discussed.

Section 5 summarized the conclusion and future work.

2. EFPI FABRICATION AND MEASUREMENT PRINCIPLE

2.1. EFPI FABRICATION

The schematic diagram of the EFPI used in the experiment is shown in Figure 2.1. The EFPI sensor consists of two pieces of single-mode fibers (SMFs) and a small section of silica capillary tube. The tube serves as the cavity of EFPI with the interface between tube and the two pieces of fibers as reflectors. The fabrication of EFPI follows several steps. First, the ends of a piece of SMF (Corning SMF-28) and silica capillary tube are both cleaved by the fiber cleaver (Sumitomo FC-6S fiber cleaver) and spliced together using the optical fiber fusion splicer (Sumitomo type-36 fusion splicer). The outer diameter and inner diameter of the capillary tube are 125 microns and 55.1 microns, respectively. Then by the help of a microscope, the capillary tube is cleaved that only tens of microns tube are left on the end of SMF. At last another piece of SMF is cleaved and spliced with the capillary tube. It should be noted that the end of the SMF needs to be broken by hand to reduce the reflection from the end of the fiber. The microscope image of EFPI sensor is shown in Figure.2.2.

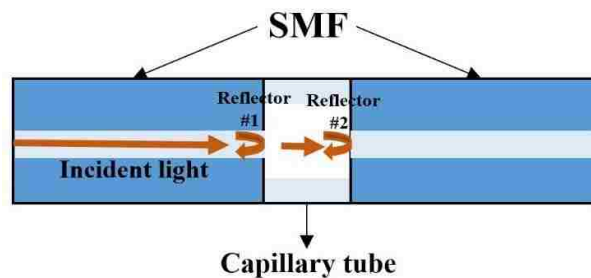


Figure 2.1. The schematic diagram of EFPI sensor

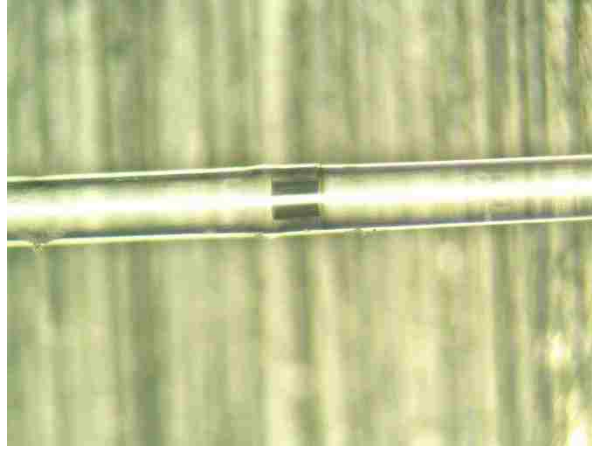


Figure 2.2. The microscope image of EFPI sensor

2.2. EFPI MEASUREMENT PRINCIPLE

The two reflected beams will interfere each other, and the magnitude of the interference spectrum can be determined by:

$$I(\lambda) = I_0(\lambda) (R_1 + R_2 + 2\sqrt{R_1 R_2} \cos \varphi) \quad (2)$$

where λ is the wavelength, $I_0(\lambda)$ is the power distribution of the incident light, R_1 and R_2 are the reflectivity of two reflectors, respectively, φ is the phase difference between two reflected beams, which is given by:

$$\varphi = \frac{4\pi L}{\lambda} \quad (3)$$

where L is the length of the capillary tube. When φ is a multiple of 2π , the constructive interference is achieved, and the condition can be expressed as:

$$\lambda = \frac{2L}{k}, k = 0, 1, 2, \dots \quad (4)$$

When the EFPI sensor is heated, due to the thermal expansion effect, the length of the capillary tube will change which results in the shift of the position of the peaks and the

valleys of the spectrum. It can be found in Equation (3) that the change in cavity length ΔL is proportional to the change in the constructive wavelength $\Delta\lambda$, which is given by:

$$\frac{\Delta\lambda}{\lambda_0} = \frac{\Delta L}{L_0} \quad (5)$$

where L_0 and λ_0 are the initial length for capillary tube and initial wavelength of constructive interference, respectively. The interference spectrum of an EFPI sensor is shown in Figure 2.3. Figure 2.3(a) shows the original spectrum of an EFPI sensor which has a periodic pattern according to Equation (2). And Figure 2.3(b) shows the spectra of EFPI before (blue curve) and after cavity length (red curve). A wavelength shift between two interference spectra can be clearly observed in Figure 2.3(b). By measuring the wavelength shift $\Delta\lambda$, the cavity length change then can be calculated according to Equation (5).

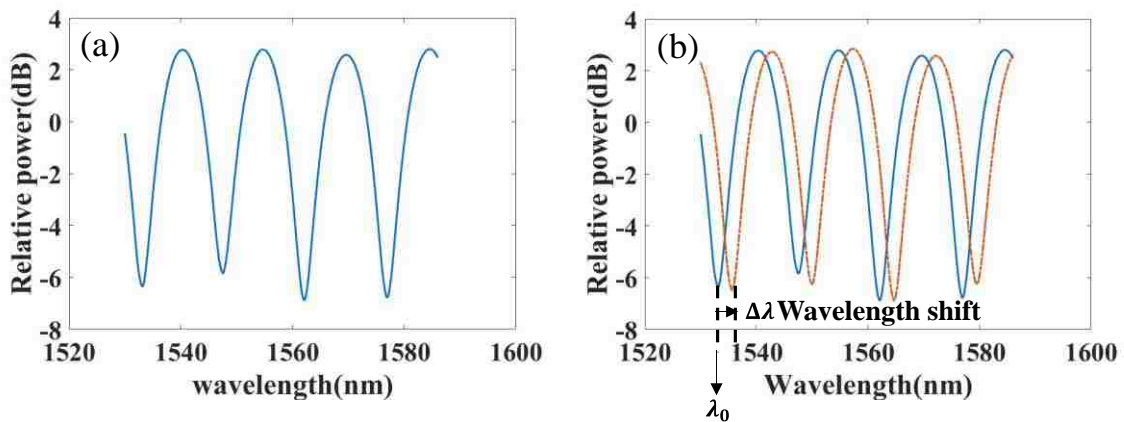


Figure 2.3. The interference spectrum of an EFPI sensor (a) Original spectrum (b) Before and after cavity length change

Without embedding, only the thermal expansion effect dominates the sensitivity of EFPI sensor. The typical coefficient of thermal expansion for fused silica is $5.5 \times 10^{-7} / ^\circ\text{C}$ so the sensitivity for EFPI sensor is about $10 \text{ pm}/^\circ\text{C}$. Considering that the OSA used in the experiment only has a 0.01 nm spatial resolution, the sensitivity for EFPI sensor is about 10°C , which can be claimed as insensitive to temperature. But after embedding, the EFPI sensor can be squeezed or stretched by copper due to the mismatch between the thermal expansion effect of copper (typical value is $1.5 \times 10^{-5} / ^\circ\text{C}$) and fused silica, which can result in extra tube length change. In conclusion, the temperature sensitivity for EFPI sensor can be enhanced after embedding.

3. OFDR MEASUREMENT PRINCIPLE

3.1. BASIC PRINCIPLE OF OFDR

The basic system structure of OFDR is shown in Figure 3.1. A highly coherent tunable laser (TLS) continuously sweep linearly as a function of time. The light from TLS is sent into an optical coupler with 50:50 split ratio and was divided into two arms: test arm and reference arm. The optical signals travel through both arms and the reflections from Rayleigh backscattering signals (RBS) from both arms will be coupled together and mix at the photodetector. The RBS signals will generate a beat signal, and the distributed sensing will be achieved by analyzing the beat spectrum converted from the detected beat signal via Fourier transform.

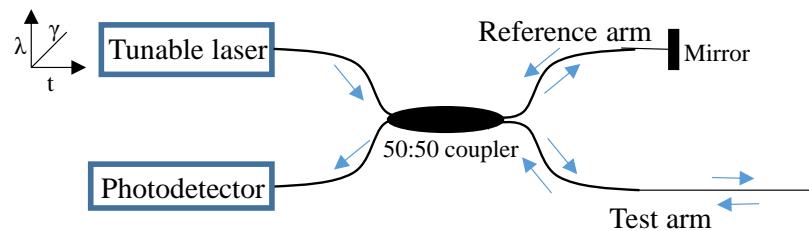


Figure 3.1. The basic principle of OFDR system

Every moment, the RBS signals generated from each position of test arm will have a beat signal with the RBS signals generated from the reference arm. Since the laser is continuously sweeping with time, the frequencies vary with the reflection location. Considering the location x of the test fiber, assuming that the length difference between

location x and the far end of reference arm to coupler is D , then the relationship between D and the beat frequency f_b can be determined as [54]:

$$D = \frac{c}{2n_o\gamma} f_b \quad (6)$$

where γ is the frequency scanning speed of the tunable laser. Here we assume that the frequency scanning speed is a constant value. It can be found that a beating signal uniquely determined by the location x at the testing arm. The magnitude and the phase information of the beating signals can be used to gauge the change of local Rayleigh scattering, which can be related to RI changes or the physical length change of optical fiber. It is worth noticing that the length difference D cannot exceed the coherence length of the tunable laser.

The theoretical spatial resolution of OFDR system can be determined as:

$$\Delta Z = \frac{c}{2n_o\Delta F} \quad (7)$$

where ΔF is the sweeping range of TLS (unit: GHz). For example, if the wavelength of TLS scans from 1530 nm to 1550 nm, ΔF is calculated to be 2500 GHz, and ΔZ is calculated to be 40 μm according to Equation (6).

3.2. NONLINEAR SWEPT

To reach a high update rate and a high spatial resolution for distributed temperature measurement, a fast TLS is highly needed. The calculation in Section 3.1 is based on the assumption that the frequency scanning speed of TLS is a constant. However, a fast TLS always have an unstable frequency sweep which increases the difficulty of detecting the weak Rayleigh scattering signals in the beat frequency domain of OFDR system. A

common method to solve the nonlinearity issue is to introduce an auxiliary interferometer to suppress the nonlinear frequency sweep of a coherent light source in an OFDR with fast tuning speed [55]. As shown in Figure 3.2 if the interference signal in the main interferometer is acquired in equal time difference, then it can be found in Equation (5) that the location information is not only related to the beat frequency. But with the auxiliary Mach-Zehnder interferometer (AZMI), the data acquisition card (DAQ) can sample the beat signal with same optical frequency difference instead of same time difference because the trigger signal generated by AZMI has same optical frequency difference. As a result, the usage of AZMI can greatly decrease the nonlinearity of the OFDR system.

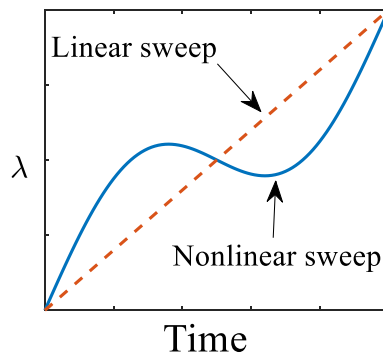


Figure 3.2. The nonlinear swept of the tunable laser

The frequency of the trigger signal generated by auxiliary interferometer can be described as:

$$f_a = \gamma \frac{n_o z}{c} \quad (8)$$

where γ is the sweeping speed of the tunable laser (unit: GHz/s); z is the path difference between two arms of the auxiliary interferometer. Since the sweeping time of one cycle is determined by the sweeping speed and the sweeping range, the data points of the interference signal in the main interferometer acquired by data acquisition system can be described as:

$$N = f_a \frac{\Delta F}{\gamma} = \frac{n_o z \Delta F}{c} \quad (9)$$

So the maximum length of FUT can be calculated as:

$$L_{\max} = \frac{N \Delta Z}{2} = \frac{z}{4} \quad (10)$$

It should be noted that the factor of 2 in Equation (9) is due to the Nyquist sampling theorem. It can be found in Equation (9) that to achieve the desired measurement range of OFDR system with an AZMI, the path difference between two arms of AZMI must be at least 4 times the measurement range.

3.3. DATA PROCESSING PROCEDURE

The temperature variation will change the optical path difference between test arm and a reference arm, which will cause some modification in the local Rayleigh backscattering. As a result, a shift in RBS will be generated. An effective method to determine the RBS introduced by temperature is cross-correlation. The signal processing procedure for temperature sensing in detail is as follows:

Step 1: Acquire the beat signal for the first time and save it as the reference signal.

The points of the acquired data can be less than the calculation result in Equation (9).

Step 2: Continuously acquire the beat signal as the measurement signal, convert both signals into beat spectra via fast Fourier transform (FFT).

Step 3: Use a sliding window (with a width ΔX) in both beat spectra to select the signal with same beat frequencies, and convert the selected data back via inverse fast Fourier transform (IFFT). Zero-padding can be applied to increase the frequency resolution in the process of IFFT.

Step 4: Apply the cross-correlation between two signals. By monitoring the cross-correlation peak shift, the temperature change can be determined.

By using cross-correlation method to get the RBS shift caused by temperature, the real spatial resolution of the OFDR system is determined by:

$$\Delta Z_1 = \Delta Z \Delta X \quad (11)$$

4. EMBEDDING PROCESS AND MEASUREMENT RESULT

4.1. EMBEDDING PROCESS

Electrodeposition was carried out to embed the optical fiber sensors. Copper sulfate solution was used as an electrolyte with Sulfuric acid. Optical fibers were non-conductive which should be made conductive to use electrodeposition to embed them into copper. The composition of the electrolyte used for electrodeposition is 41.5 gm of anhydrous copper sulfate, 7.5 mL of sulfuric acid (98%) in 345 mL De-ionized water. The electrodes used were: Superconductive copper from McMaster-Carr as cathode and Phosphor-Copper from Caswell as an anode. The surface preparation of the electrodes was done by grinding them from 60 to 1200 grade sandpapers.

The interface between the fiber and the copper was one of the important factors in sensing temperature. The interface was altered by changing the porosity at the fiber-copper interface. Three approaches were designed and implemented. First being the chemically plated fiber, a layer of copper was obtained on the fiber using electro-less/chemical plating process [60]. The fiber was hydroxylated before chemical plating by placing it in 98% sulfuric acid for 2 minutes. The chemical plating process was carried out by using three solutions, namely activating solution, sensitizing solution, and chemical plating solution. The second one was the copper painted fiber; the fiber was coated with copper paint using dip coating. Finally, for the wax interface, the fiber was coated with Natural Beeswax from McMaster-Carr before dip coating it with copper paint. After obtaining conductive layer using the previous three methods, the electrodeposition was carried out using Agilent

U8031A DC power supply with a constant current of 0.5A. The photo of the copper slide with embedded optical fiber sensor is illustrated in Figure 4.1.

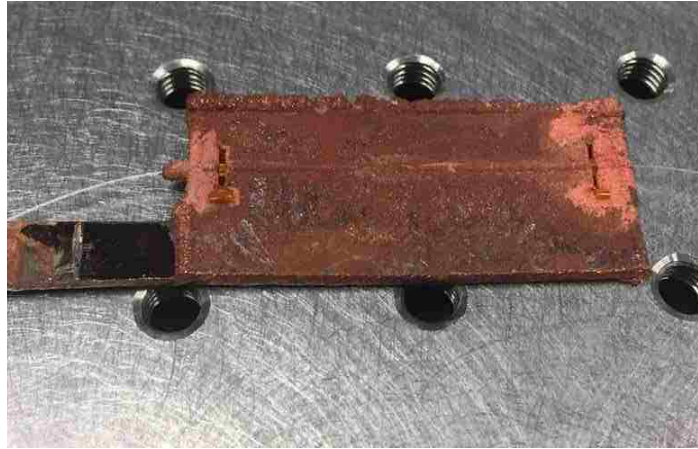


Figure 4.1. The photo of copper slide with embedded optical fiber sensor

4.2. EFPI MEASUREMENT

After embedding the sensors into the copper substrate, the samples were tested. The experiment setup is shown in Figure 4.2. The system consists of a light source, a 50/50 optical fiber coupler, an optical spectrum analyzer (OSA), a tube furnace and a sensor head. The light launched by a broadband light source (BBS, Thorlabs ASE-FL7002-C4 broadband ASE light source, 1530-1610nm) was injected into one 50% arm of the coupler and then propagates towards EFPI sensor from 1-arm. A small portion of the incident light would be reflected by the first cleaved end of SMF, while the rest of light would travel through the capillary tube and be reflected by the second interface. The reflected beams would be coupled into the coupler again and be detected by an OSA (Ando AQ6317B

optical spectrum analyzer) through another 50% arm. The OSA was connected to a laptop and controlled by MATLAB to record the reflection spectrums. For the parameters of OSA, the number of points was set to 2001; the recorded wavelength range was set from 1530 nm to 1600 nm, and the resolution of OSA was set to 0.5 nm.

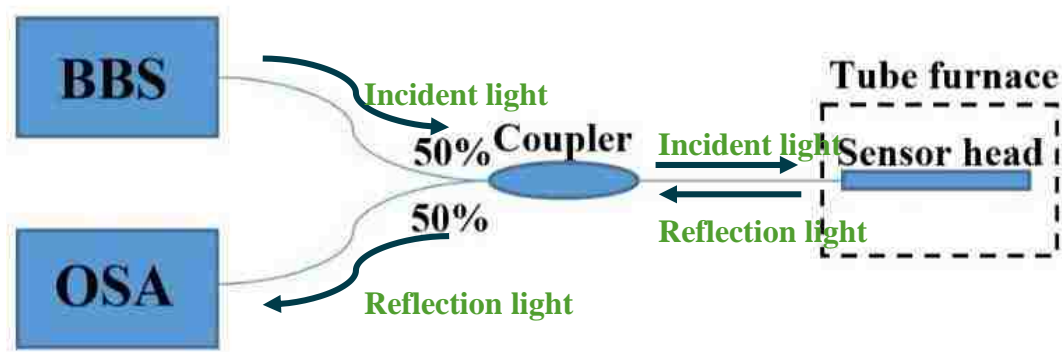


Figure 4.2. The schematic diagram of the setup of EFPI sensor calibration experiment

Figure 4.3 shows the results of EFPI temperature measurement for different cases. The measured temperature range was from 100 °C to 700 °C. And the reflection spectrum of EFPI was recorded every 50 °C to analyze the spectrum shift. Table 4.1 summarizes the sensitivities of EFPI sensors with different embedding method against temperature. For the EFPI sensor without embedding, the measurement result shows the spectral shift changes linearly with the temperature, which matches the theoretical calculation in Equation (5). The sensitivity for EFPI sensor is 10 pm/°C. For embedded EFPI sensors with copper paint, the sensitivity of the sensor is 13 pm/ °C from 100 °C to 350 °C, which is in the range of the sensitivity of EFPI sensor without embedding. From 350 °C to 700 °C, the sensitivity of

sensor dramatically increases to $44.8 \text{ pm}/^\circ\text{C}$. For EFPI sensor with chemically plating, the sensitivity from $100 \text{ }^\circ\text{C}$ to $200 \text{ }^\circ\text{C}$ is $50.7 \text{ pm}/^\circ\text{C}$. From $200 \text{ }^\circ\text{C}$ to $350 \text{ }^\circ\text{C}$, the spectrum shifts in the opposite direction, and the sensitivity is $-40.6 \text{ nm}/^\circ\text{C}$. And from $350 \text{ }^\circ\text{C}$, the sensitivity of the sensor is $50.4 \text{ pm}/^\circ\text{C}$ which is similar to the EFPI sensor with copper paint. After $650 \text{ }^\circ\text{C}$ the reflection spectrum of EFPI sensor is deformed, and the power of the reflection power greatly decreases. The change is irreversible, and the spectrum shift cannot be read in this case. For embedded EFPI sensor with a wax coating, the relationship between temperature and spectrum shift from $100 \text{ }^\circ\text{C}$ to $700 \text{ }^\circ\text{C}$ is always linear. The sensitivity of the sample is $60 \text{ pm}/^\circ\text{C}$.

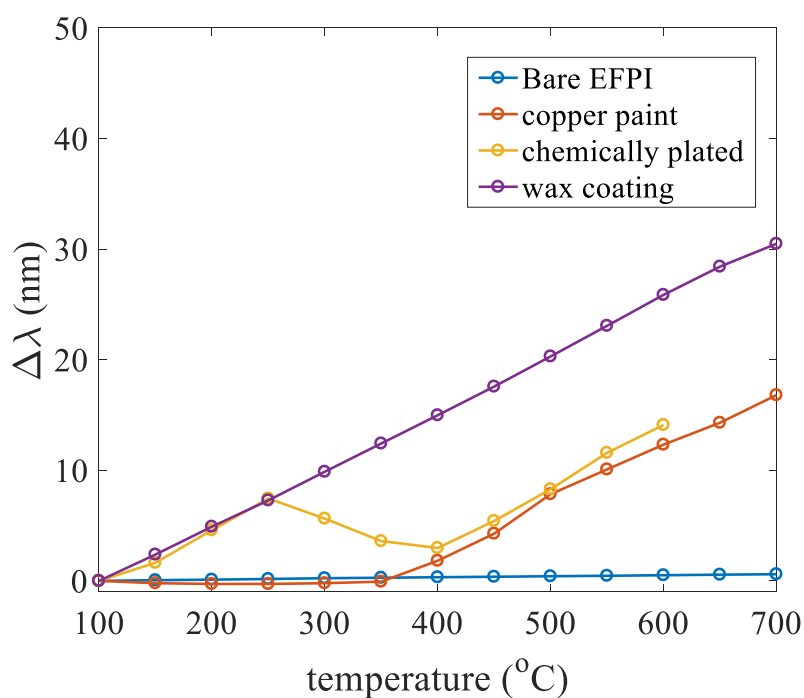


Figure 4.3. The spectral shift of EFPI sensors with different coating as a function of temperature

Table 4.1. EFPI sensitivity with different coating in different temperature

Interface	Sensitivity (pm/°C)		
	RT – 250°C	250 – 350°C	350– 700°C
Bare fiber	1	1	1
Chemical plated	1.3	1.3	44.8
Copper paint	57.4	-40.6	50.4
Wax	60	60	60

As mentioned in Section 2.2, due to the mismatch of the CTE of fused silica and copper, the optical fiber could be squeezed by copper, and the sensitivity of EFPI can be greatly enhanced. However, the optical fiber cannot survive too much strain (normally 1%). For embedded EFPI sensor with copper paint, when the temperature was low, the gap between copper and optical fiber remained so the EFPI sensor was not squeezed. When the temperature increased, the gap became smaller and finally EFPI sensor was squeezed, and the sensitivity was enhanced. For the embedded EFPI sensor with chemical plating, the sensor shows high sensitivity at low temperature, which indicates that the sensor had been squeezed after embedding. But from 200 °C to 350 °C, the spectrum shifts in opposite direction, so the sensitivity becomes negative. One reason was that the coating material vaporized during the experiment which results in the de-bonding between the optical fiber and the copper. After 350 °C due to the thermal expansion the optical fiber was squeezed

again and the sensitivity increases. After 600 °C, the spectrum is deformed because the cavity of EFPI sensor was broken due to the strain introduced by copper. For embedded EFPI sensor with wax, the purpose of using wax sample was to create a gap between EFPI sensor and copper, but the sensitivity of the sensor was surprisingly enhanced, and good linearity between temperature and spectrum shift was achieved. The EFPI experiment shows that coating a thin layer of wax before embedding can protect the embedded sensor from large strain as well as improve the performance of the sensor.

An experiment was conducted for monitoring the temperature change of the mold during casting of aluminum to verify if the sensor can response to the fast temperature change. The photos of the casting mold are illustrated in Figure 4.4(a) and Figure 4.4(b). The copper slide with the embedded EFPI sensor was inserted to the side of the mold. To protect the lead-in optical fiber, the ceramic paste was used to stick the optical fiber to a steel rod. A thermocouple was also placed inside the mold near the copper slide as a reference. Since the temperature change rate in casting experiment was expected to be faster than in calibration experiment, several parameters of OSA was adjusted to increase the scanning speed. The number of points and the wavelength span of OSA was decreased to 501 and 15 nm, respectively. During the aluminum casting experiment, the melted aluminum was poured into the mold, and the spectrum of OSA and the temperature data of thermocouple were both recorded every second. The total measurement time was 700 seconds.

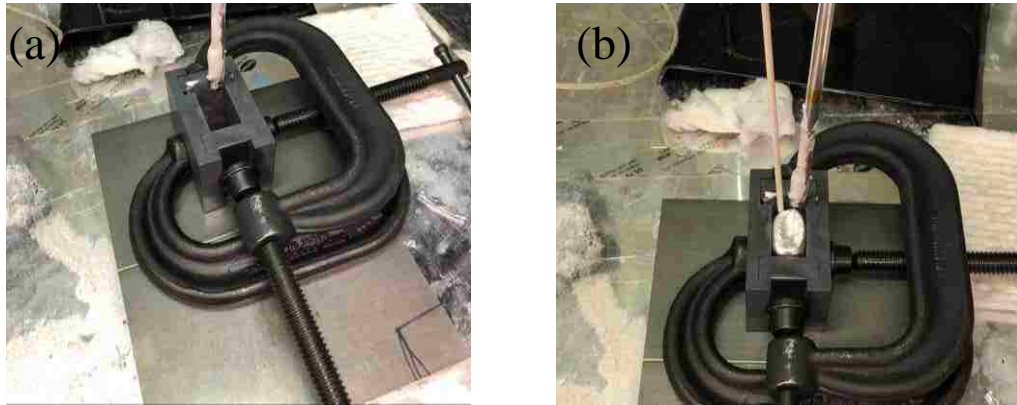


Figure 4.4. The photo of the casting mold (a) Before experiment (b) After aluminum casting experiment

The recorded temperature change of thermocouple and the calculated temperature change of EFPI sensor as a function of time are illustrated in Figure 4.5. It is shown in Figure 4.5 that the temperature of the mold was increased very fast in a few seconds after the melted aluminum was poured into the mold, and then the temperature was decreased following an exponential decay. The temperature change of the thermocouple and the EFPI sensor shows a similar trend, indicating that the embedded EFPI sensor can achieve fast response time. It can also be found in Figure 4.5 that the highest temperature recorded by thermocouple was much higher than temperature recorded by EFPI sensor (about 250 °C higher). The reason for the difference is that the melted aluminum did not fill the whole mold. In Figure 4.4(b) several gaps between the aluminum and mold can be observed. As a result, the thermocouple and the EFPI sensor may not survive with the same temperature. But with the calibration experiment result, it still can be proved that the embedded EFPI sensor can survive at least 600 °C with fast response.

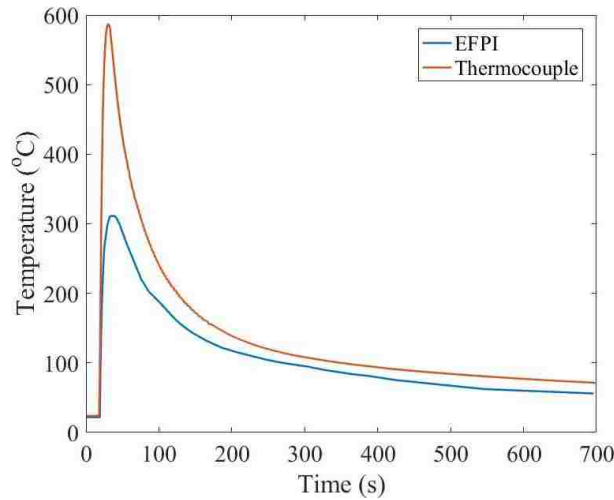


Figure 4.5. The temperature response of the EFPI sensor and thermocouple as a function of time

4.3. OFDR MEASUREMENT

After EFPI experiment, 4 cm optical fiber was embedded into the copper slide, and the embedded optical fiber was connect to the OFDR experiment setup for temperature sensing. The experimental setup of OFDR system and the measurement apparatus are illustrated in Figure 4.6. The light from TLS (Agilent 8164A Lightwave Measurement System) was split into two paths by a coupler. One path led to the AZMI to generate the trigger signal for DAQ. The other path led to the main interferometer. The main interferometer was also an M-Z interferometer and the light was divided into reference arm and test arm. For the reference arm, a polarization controller was set in the reference arm of the main interferometer to optimize the interference signal. For the test arm, the optical signal will pass through a circulator into the fiber under test (FUT). And the RBS signal will travel back through FUT to the circulator again. The signal of the reference arm and the RBS signal will be coupled by another coupler and interfere. Then the interference

signal will be detected and recorded. The balanced photodetectors are both used in the main interferometer and AZMI to reduce the common-mode noise. The embedded fiber is put into the middle of the tube furnace. The tuning speed of TLS was set to 40 nm/s and the tuning range of TLS was set to 20 nm (1520 nm-1540 nm). During the data processing, the size of the window was set to 250, corresponding to the spatial resolution of 1 cm.

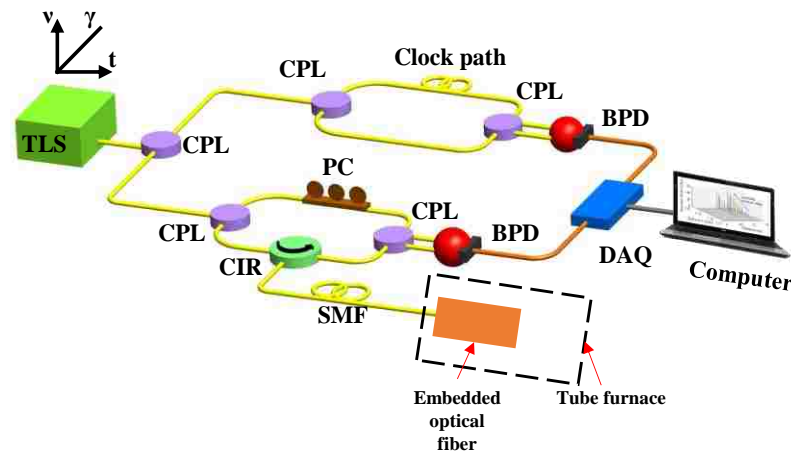


Figure 4.6. The schematic diagram of the OFDR system and the measurement setup

First, the copper slide with embedded optical fiber was annealed at 500 °C. The RBS spectral shift curves of the optical fiber during the heating process at 12 different temperature are shown in Figure 4.7. The frequency shift along whole FUT was recorded. Here, only the RBS shift data from 4.85 m to 5.35 m of FUT is presented in Figure 4.6 because only this part of FUT was placed into the tube furnace. The RBS spectral shift of embedded optical fiber is demonstrated between two dash lines. Since the temperature in the center of tube furnace was much higher than the temperature on both sides, Figure 4.7

shows that optical fiber in the middle of tube furnace has higher RBS spectral shift. It is worth noticing that at the beginning of the heating process, the RBS spectral shift was decreasing from the optical fiber without embedding to embedded optical fiber. The reason is that the copper slide was placed into a glass tube. As a result the lead-in optical fiber near the copper slide was hung in the air. After 450 °C, the RBS shift of embedded optical fiber increased faster than before and at 500 °C the embedded optical had larger RBS shift than optical fiber without embedding. This indicates that the copper slides squeezed the embedded optical fiber at high temperature. Figure 4.8(a) and 4.8(b) shows the relationship between temperature and RBS shift points of embedded and normal optical fiber. Figure 4.8(a) shows that for normal optical fiber, the relationship the relationship between temperature and RBS shift points had good linearity. The slope of curve fitting result of Figure 4.7(a) is 17.3 points/°C, and R-square is 0.9997. While in Figure 4.8(b), the slope of the curve increased at 450 °C. The results matched the EFPI experimental result that the optical fiber would be squeezed in high temperature after embedding.

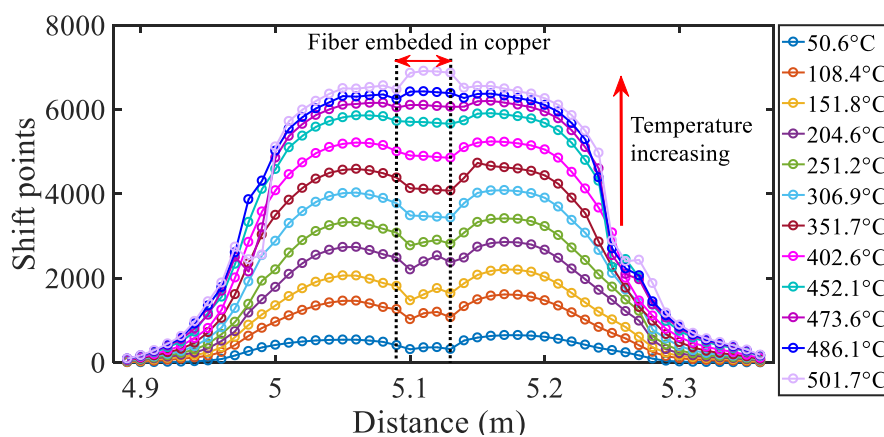


Figure 4.7. The RBS shifts along the optical fiber inside the furnace in different temperature during heating of annealing process

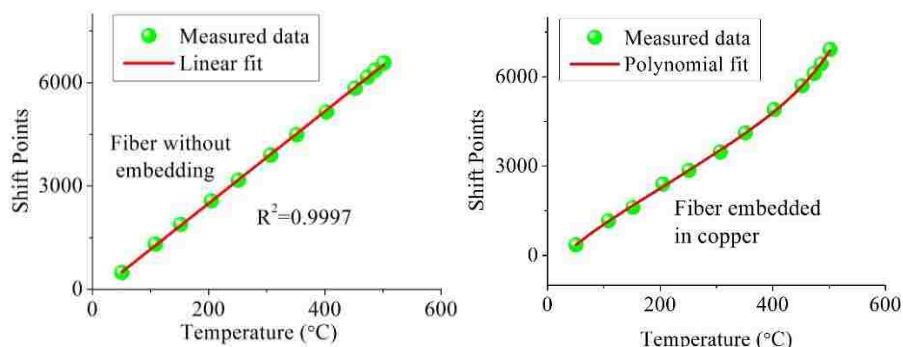


Figure 4.8. The RBS shift points of the optical fiber as a function of temperature during heating of annealing process (a) Unembedded optical fiber (b) Embedded optical fiber

After annealing for 15 minutes, the copper slide was cooled down. And Figure 4.9 shows the RBS spectral shift during the cooling process. It is obvious that at the beginning of the cooling process the embedded optical fiber had larger RBS spectral shift. And when the temperature was continuously decreasing, the rate of the spectral shift was also decreasing. Figure 4.9 shows the relationship between temperature and RBS spectral shift point. Figure 4.9 shows that for normal optical fiber, the relationship between temperature and RBS shift point still kept good linearity. Meanwhile, the rate of RBS shift for embedded optical fiber was around 2 times larger than normal optical fiber because the thermo-optic effect of the optical fiber ($6.1 \times 10^{-6} / ^\circ\text{C}$) and thermal expansion effect of copper both contributed to the RBS shift. The rate of RBS shift decreased in low temperature, which indicated that de-bonding between the copper slide and optical fiber happened during the cooling process.

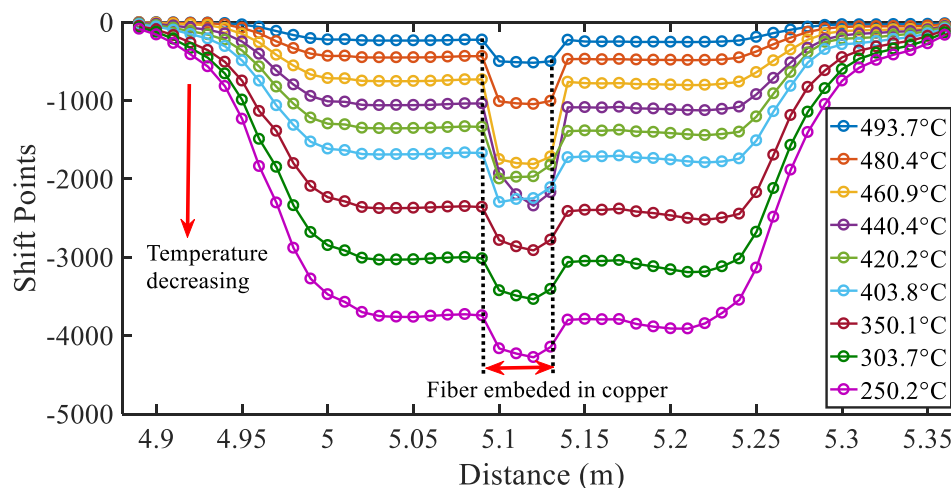


Figure 4.9. The RBS shifts along the optical fiber inside the furnace in different temperature during cooling of annealing process

The embedded optical fiber was tested again after cooling process. In this experiment, the embedded optical fiber was heated to 700 °C. Figure 4.10 shows that optical fiber in the middle of tube furnace had higher RBS spectral shift. Comparing with the heating process of annealing, the rate of RBS spectral shift also changed with temperature, and this change followed the similar trend of the heating process of annealing. Figure 4.11(a) and 4.11(b) shows the relationship between temperature and RBS spectral shift point. For normal optical fiber, the relationship between temperature and RBS shift point still kept good linearity. For the embedded optical fiber, the RBS shift was still smaller than unembedded optical fiber, and with the temperature increasing, the RBS shift increased at a faster rate compared with unembedded optical fiber.

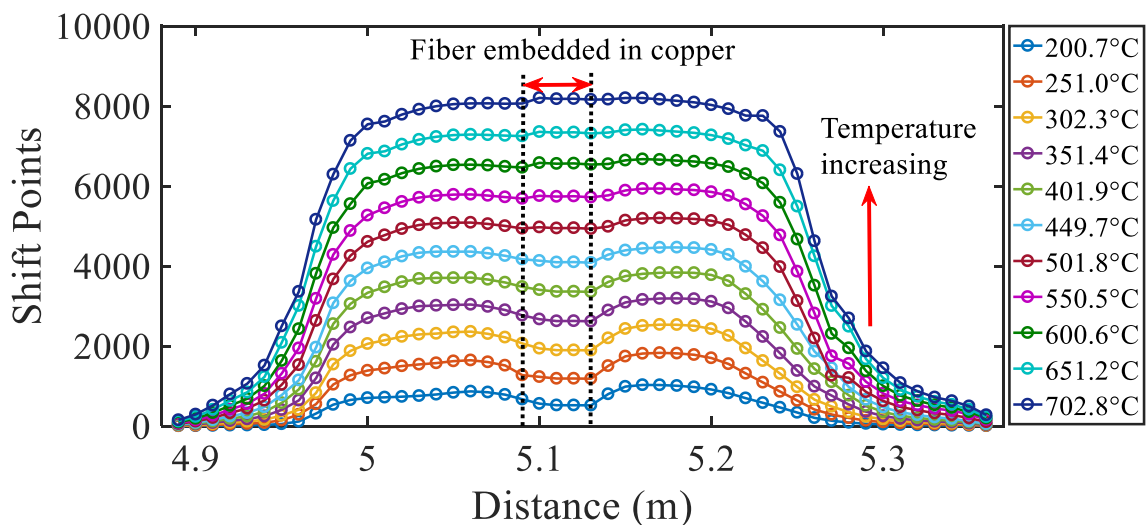


Figure 4.10. The RBS shifts along the optical fiber inside the furnace in different temperature during heating experiment

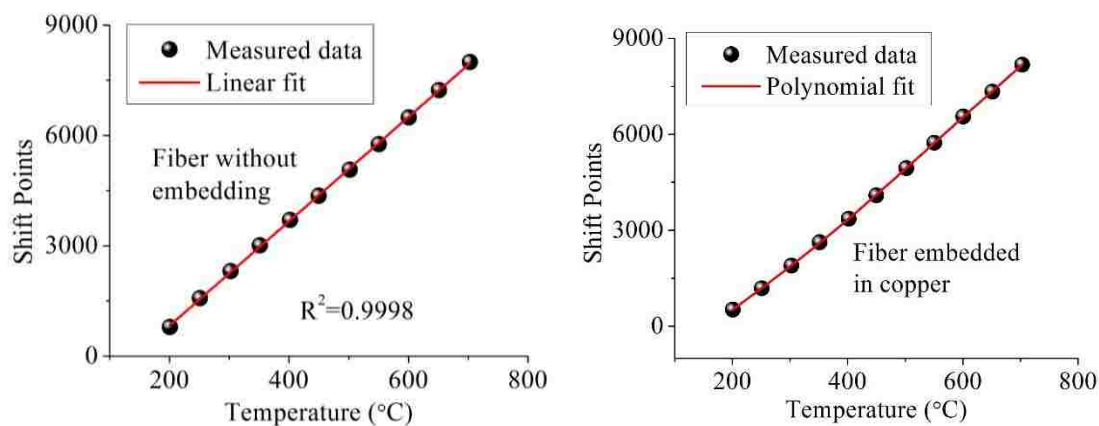


Figure 4.11. The RBS shift points of the optical fiber as a function of temperature during heating experiment (a) Unembedded optical fiber (b) Embedded optical fiber

The RBS shift of optical fiber when the optical fiber was cooled down from 700 °C is shown in Figure 4.12. The RBS shift of embedded optical fiber sensors was still larger than the unembedded optical fiber, which is similar to the result during the cooling process

of annealing. In Figure 4.13(a) and (b), compared with the slope of the linear fitting results of the optical fiber with and without embedding, it can be found that the embedded optical fiber has higher temperature sensitivity than unembedded optical fiber. And in high temperature where the de-bonding would not happen, the RBS shift of embedded optical fiber showed good linearity. The optical fiber was broken during the experiment because in high temperature the polymer coating of optical fiber would be burnt off, and also the mechanical strength of fused silica would decrease after it was heated in high temperature.

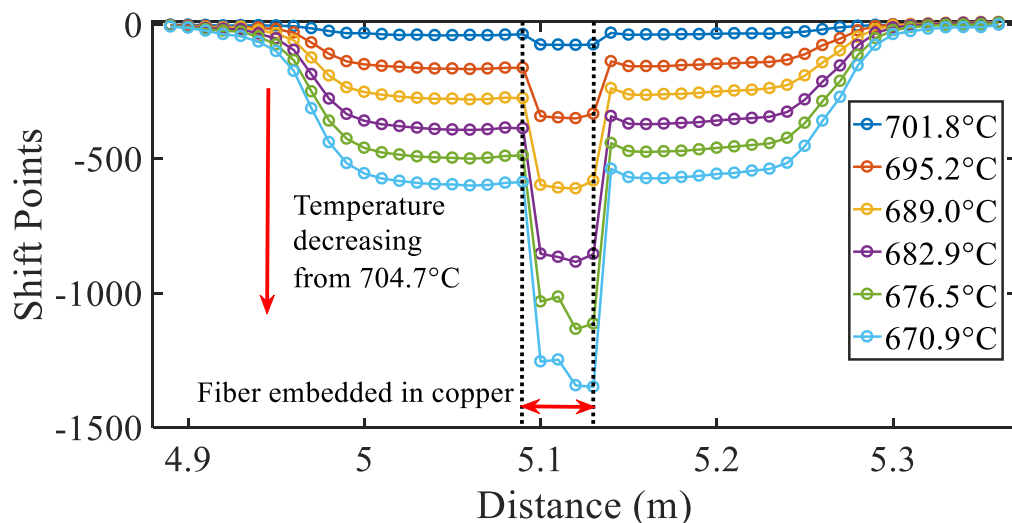


Figure 4.12. The RBS shifts along the optical fiber inside the furnace in different temperature during cooling experiment

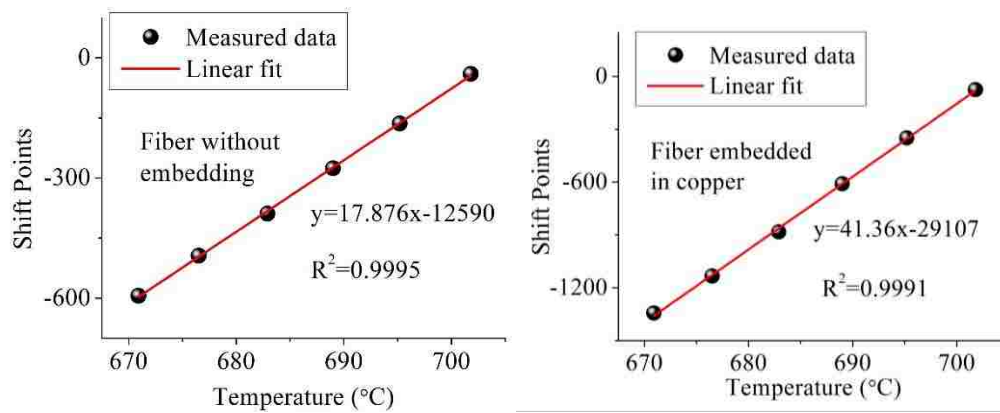


Figure 4.13. The RBS shift points of the optical fiber as a function of temperature during cooling experiment (a) Unembedded optical fiber (b) Embedded optical fiber

5. CONCLUSION AND FUTURE WORK

In this thesis, we successfully developed optical fiber point sensor (EFPI) and optical fiber distributed sensor (OFDR) and embedded them inside the copper slides using electrodeposition for high-temperature sensing. The fabrication and the working principle of EFPI sensor were introduced in this thesis. To investigate the best method to create a gap between optical fiber sensor and the copper slide, three coating methods were applied to coat the EFPI sensors before embedding. And the EFPI sensors with different coating method were calibrated separately in the high-temperature experiments. Among them, the EFPI sensor with wax coating not only could survive in high temperature, but also its sensitivity was surprisingly enhanced for more than 30 times. An aluminum casting experiment was also conducted to verify the time response of the EFPI sensor, which showed the practicability of EFPI sensor. The system structure and the sensing principle of OFDR system were also introduced in this thesis. And a preliminary calibration experiment of OFDR system with embedded optical fiber was achieved, showing the optical fiber can survive in 700 °C and the optical fiber distributed sensing can be achieved.

During the project, the repeatability of optical fiber sensors was not good. The main reason for the problem is that the polymer coating of the optical fiber will be burned off in high temperature during the test, and also the mechanical strength of the optical fiber will decrease after several heating and cooling cycles. As a result, the lead-in optical fiber was always broken at the boundary of the lead-in optical fiber and the copper slide. So a better way to protect the lead-in optical fiber needs to be developed. And although wax coating can enhance the sensitivity of EFPI sensor with linear response, in OFDR calibration test

the sensitivity was not constant. The interaction between the optical fiber sensors and copper still need to be investigated. And finally, we will develop a mold with embedded optical fiber sensors that can measure the temperature distribution of the whole mold.

BIBLIOGRAPHY

- [1] C. A. Santos, A. Garcia, C. R. Frick, and J. A. Spim, "Evaluation of heat transfer coefficients along the secondary cooling zones in the continuous casting of steel billets," *Inverse Problems in Science and Engineering*, vol. 14, pp. 687-700, 2006/09/01 2006.
- [2] S. Singh and K. Blazek, "Heat transfer and skin formation in a continuous-casting mold as a function of steel carbon content," *JOM*, vol. 26, pp. 17-27, 1974.
- [3] Y. Kashiwaya, C. E. Cicutti, and A. W. Cramb, "An investigation of the crystallization of a continuous casting mold slag using the single hot thermocouple technique," *ISIJ international*, vol. 38, pp. 357-365, 1998.
- [4] J. Cho, H. Shibata, T. Emi, and M. Suzuki, "Thermal resistance at the interface between mold flux film and mold for continuous casting of steels," *ISIJ international*, vol. 38, pp. 440-446, 1998.
- [5] T. Nakano, T. Kishi, K. Koyama, T. KOMAI, and S. NAITOH, "Mold powder technology for continuous casting of aluminum-killed steel," *Transactions of the Iron and Steel Institute of Japan*, vol. 24, pp. 950-956, 1984.
- [6] B. Lee, "Review of the present status of optical fiber sensors," *Optical fiber technology*, vol. 9, pp. 57-79, 2003.
- [7] A. Bahrapour, A. Moosavi, M. Bahrapour, and L. Safaei, "Spatial resolution enhancement in fiber Raman distributed temperature sensor by employing ForWaRD deconvolution algorithm," *Optical Fiber Technology*, vol. 17, pp. 128-134, 2011.
- [8] K. Bohnert, P. Gabus, J. Nehring, and H. Brandle, "Temperature and vibration insensitive fiber-optic current sensor," *Journal of Lightwave Technology*, vol. 20, p. 267, 2002.
- [9] H. Y. Choi, K. S. Park, S. J. Park, U.-C. Paek, B. H. Lee, and E. S. Choi, "Miniature fiber-optic high temperature sensor based on a hybrid structured Fabry-Perot interferometer," *Optics letters*, vol. 33, pp. 2455-2457, 2008.
- [10] A. Ghazanfari, W. Li, M. C. Leu, Y. Zhuang, and J. Huang, "Advanced ceramic components with embedded sapphire optical fiber sensors for high temperature applications," *Materials & Design*, vol. 112, pp. 197-206, 2016.
- [11] T. Wei, Y. Han, Y. Li, H.-L. Tsai, and H. Xiao, "Temperature-insensitive miniaturized fiber inline Fabry-Perot interferometer for highly sensitive refractive index measurement," *Optics Express*, vol. 16, pp. 5764-5769, 2008.

- [12] Y. Du, Y. Chen, Y. Zhuang, C. Zhu, F. Tang, and J. Huang, "Probing nanostrain via a mechanically designed optical fiber interferometer," *IEEE Photonics Technology Letters*, vol. 29, pp. 1348-1351, 2017.
- [13] D.-W. Duan, Y.-j. Rao, Y.-S. Hou, and T. Zhu, "Microbubble based fiber-optic Fabry–Perot interferometer formed by fusion splicing single-mode fibers for strain measurement," *Applied optics*, vol. 51, pp. 1033-1036, 2012.
- [14] C.-L. Lee, W.-C. Shih, J.-M. Hsu, and J.-S. Horng, "Asymmetrical dual tapered fiber Mach-Zehnder interferometer for fiber-optic directional tilt sensor," *Optics Express*, vol. 22, pp. 24646-24654, 2014/10/06 2014.
- [15] E. Li, "Sensitivity-enhanced fiber-optic strain sensor based on interference of higher order modes in circular fibers," *IEEE Photonics Technology Letters*, vol. 19, pp. 1266-1268, 2007.
- [16] H. Murayama, D. Wada, and H. Igawa, "Structural health monitoring by using fiber-optic distributed strain sensors with high spatial resolution," *Photonic Sensors*, vol. 3, pp. 355-376, 2013.
- [17] Y. Du, S. Jothibas, Y. Zhuang, C. Zhu, and J. Huang, "Rayleigh backscattering based macrobending single mode fiber for distributed refractive index sensing," *Sensors and Actuators B: Chemical*, vol. 248, pp. 346-350, 2017.
- [18] W. Liang, Y. Huang, Y. Xu, R. K. Lee, and A. Yariv, "Highly sensitive fiber Bragg grating refractive index sensors," *Applied physics letters*, vol. 86, p. 151122, 2005.
- [19] P. Lu, L. Men, K. Sooley, and Q. Chen, "Tapered fiber Mach–Zehnder interferometer for simultaneous measurement of refractive index and temperature," *Applied Physics Letters*, vol. 94, p. 131110, 2009.
- [20] Z. Tian, S. S. Yam, and H.-P. Loock, "Refractive index sensor based on an abrupt taper Michelson interferometer in a single-mode fiber," *Optics letters*, vol. 33, pp. 1105-1107, 2008.
- [21] H. Bao, X. Dong, C. Zhao, L.-Y. Shao, C. C. Chan, and P. Shum, "Temperature-insensitive FBG tilt sensor with a large measurement range," *Optics Communications*, vol. 283, pp. 968-970, 2010.
- [22] G. T. Kanellos, G. Papaioannou, D. Tsiokos, C. Mitrogiannis, G. Nianios, and N. Pleros, "Two dimensional polymer-embedded quasi-distributed FBG pressure sensor for biomedical applications," *Optics express*, vol. 18, pp. 179-186, 2010.
- [23] N. A. Mohammed, T. A. Ali, M. H. Aly, and O. Member, "Evaluation and performance enhancement for accurate FBG temperature sensor measurement with different apodization profiles in single and quasi-distributed DWDM systems," *Optics and Lasers in Engineering*, vol. 55, pp. 22-34, 2014.

- [24] B.-J. Peng, Y. Zhao, Y. Zhao, and J. Yang, "Tilt sensor with FBG technology and matched FBG demodulating method," *IEEE Sensors Journal*, vol. 6, pp. 63-66, 2006.
- [25] X. Chen, F. Shen, Z. Wang, Z. Huang, and A. Wang, "Micro-air-gap based intrinsic Fabry-Perot interferometric fiber-optic sensor," *Applied optics*, vol. 45, pp. 7760-7766, 2006.
- [26] G. Cranch, C. Kirkendall, K. Daley, S. Motley, A. Bautista, J. Salzano, *et al.*, "Large-scale remotely pumped and interrogated fiber-optic interferometric sensor array," *IEEE Photonics Technology Letters*, vol. 15, pp. 1579-1581, 2003.
- [27] B. H. Lee, Y. H. Kim, K. S. Park, J. B. Eom, M. J. Kim, B. S. Rho, *et al.*, "Interferometric fiber optic sensors," *Sensors*, vol. 12, pp. 2467-2486, 2012.
- [28] B. Zhang and M. Kahrizi, "High-temperature resistance fiber Bragg grating temperature sensor fabrication," *IEEE Sensors Journal*, vol. 7, pp. 586-591, 2007.
- [29] H.-F. Pei, J.-H. Yin, H.-H. Zhu, C.-Y. Hong, W. Jin, and D.-S. Xu, "Monitoring of lateral displacements of a slope using a series of special fibre Bragg grating-based in-place inclinometers," *Measurement Science and Technology*, vol. 23, p. 025007, 2012.
- [30] H. Fu, H. Liu, W. Chung, and H. Tam, "A novel fiber Bragg grating sensor configuration for long-distance quasi-distributed measurement," *IEEE sensors Journal*, vol. 8, pp. 1598-1602, 2008.
- [31] B.-O. Guan, H.-Y. Tam, X.-M. Tao, and X.-Y. Dong, "Simultaneous strain and temperature measurement using a superstructure fiber Bragg grating," *IEEE Photonics Technology Letters*, vol. 12, pp. 675-677, 2000.
- [32] D. Lieftucht, M. Reifferscheid, T. Schramm, A. Krasilnikov, and D. Kirsch, "HD Mold—A new Fiber-Optical-based Mold Monitoring System," *Iron & Steel Technology*, pp. 87-95, 2013.
- [33] L. Amaral, O. Frazão, J. Santos, and A. L. Ribeiro, "Fiber-optic inclinometer based on taper Michelson interferometer," *IEEE Sensors Journal*, vol. 11, pp. 1811-1814, 2011.
- [34] X. Dong, H. Tam, and P. Shum, "Temperature-insensitive strain sensor with polarization-maintaining photonic crystal fiber based Sagnac interferometer," *Applied Physics Letters*, vol. 90, p. 151113, 2007.
- [35] H. Fu, H. Tam, L.-Y. Shao, X. Dong, P. Wai, C. Lu, *et al.*, "Pressure sensor realized with polarization-maintaining photonic crystal fiber-based Sagnac interferometer," *Applied optics*, vol. 47, pp. 2835-2839, 2008.

- [36] Y. Huang, T. Wei, Z. Zhou, Y. Zhang, G. Chen, and H. Xiao, "An extrinsic Fabry–Perot interferometer-based large strain sensor with high resolution," *Measurement science and technology*, vol. 21, p. 105308, 2010.
- [37] V. Machavaram, R. Badcock, and G. Fernando, "Fabrication of intrinsic fibre Fabry–Perot sensors in silica fibres using hydrofluoric acid etching," *Sensors and Actuators A: Physical*, vol. 138, pp. 248-260, 2007.
- [38] Y.-J. Rao, M. Deng, D.-W. Duan, X.-C. Yang, T. Zhu, and G.-H. Cheng, "Micro Fabry-Perot interferometers in silica fibers machined by femtosecond laser," *Optics express*, vol. 15, pp. 14123-14128, 2007.
- [39] T. Wei, Y. Han, H.-L. Tsai, and H. Xiao, "Miniaturized fiber inline Fabry-Perot interferometer fabricated with a femtosecond laser," *Optics letters*, vol. 33, pp. 536-538, 2008.
- [40] X. Zhou and Q. Yu, "Wide-range displacement sensor based on fiber-optic Fabry–Perot interferometer for subnanometer measurement," *IEEE sensors journal*, vol. 11, pp. 1602-1606, 2011.
- [41] Y.-J. Rao, "Recent progress in fiber-optic extrinsic Fabry–Perot interferometric sensors," *Optical Fiber Technology*, vol. 12, pp. 227-237, 2006.
- [42] C. Zhu, Y. Chen, Y. Du, Y. Zhuang, F. Liu, R. E. Gerald, *et al.*, "A Displacement Sensor With Centimeter Dynamic Range and Submicrometer Resolution Based on an Optical Interferometer," *IEEE Sensors Journal*, vol. 17, pp. 5523-5528, 2017.
- [43] H.-N. Li, D.-S. Li, and G.-B. Song, "Recent applications of fiber optic sensors to health monitoring in civil engineering," *Engineering structures*, vol. 26, pp. 1647-1657, 2004.
- [44] X. Bao and L. Chen, "Recent progress in distributed fiber optic sensors," *Sensors*, vol. 12, pp. 8601-8639, 2012.
- [45] G. Bolognini, J. Park, M. A. Soto, N. Park, and F. Di Pasquale, "Analysis of distributed temperature sensing based on Raman scattering using OTDR coding and discrete Raman amplification," *Measurement Science and Technology*, vol. 18, p. 3211, 2007.
- [46] D. Iida and F. Ito, "Detection sensitivity of Brillouin scattering near Fresnel reflection in BOTDR measurement," *Journal of Lightwave Technology*, vol. 26, pp. 417-424, 2008.
- [47] Y. Lu, T. Zhu, L. Chen, and X. Bao, "Distributed vibration sensor based on coherent detection of phase-OTDR," *Journal of lightwave Technology*, vol. 28, pp. 3243-3249, 2010.

- [48] H. Ohno, H. Naruse, M. Kihara, and A. Shimada, "Industrial applications of the BOTDR optical fiber strain sensor," *Optical fiber technology*, vol. 7, pp. 45-64, 2001.
- [49] S. Z. Yan and L. S. Chyan, "Performance enhancement of BOTDR fiber optic sensor for oil and gas pipeline monitoring," *Optical Fiber Technology*, vol. 16, pp. 100-109, 2010.
- [50] Z. Zhang and X. Bao, "Distributed optical fiber vibration sensor based on spectrum analysis of Polarization-OTDR system," *Optics express*, vol. 16, pp. 10240-10247, 2008.
- [51] M. Wegmuller, J. Von Der Weid, P. Oberson, and N. Gisin, "High resolution fiber distributed measurements with coherent OFDR," in *Proc. ECOC'00*, 2000, p. 109.
- [52] H. Murayama, K. Kageyama, K. Uzawa, K. Ohara, and H. Igawa, "Strain monitoring of a single-lap joint with embedded fiber-optic distributed sensors," *Structural Health Monitoring*, vol. 11, pp. 325-344, 2012.
- [53] S. Wang, X. Fan, Q. Liu, and Z. He, "Distributed fiber-optic vibration sensing based on phase extraction from time-gated digital OFDR," *Optics express*, vol. 23, pp. 33301-33309, 2015.
- [54] K. Tsuji, K. Shimizu, T. Horiguchi, and Y. Koyamada, "Coherent optical frequency domain reflectometry using phase-decorrelated reflected and reference lightwaves," *Journal of lightwave technology*, vol. 15, pp. 1102-1109, 1997.
- [55] T.-J. Ahn, J. Y. Lee, and D. Y. Kim, "Suppression of nonlinear frequency sweep in an optical frequency-domain reflectometer by use of Hilbert transformation," *Applied optics*, vol. 44, pp. 7630-7634, 2005.

VITA

Yiyang Zhuang was born on July 16, 1992. He obtained his bachelor degree in the school of Engineering Management of Nanjing University in June 2014. In August 2015 he joined the graduate program in the Department of Electrical and Computer Engineering at Missouri University of Science and Technology. His research interest included fiber optic sensors, microwave photonics, and coaxial cable sensors. He received a Master of Science in Electrical Engineering from Missouri University of Science and Technology in May 2018.